Fabrication and measurements of hybrid Nb/Al Josephson junctions and flux qubits with π-shifters

A V Shcherbakova[1]**, K G Fedorov**[1,2]**, K V Shulga**[2,3]**, V V Ryazanov**[2,3,4]**,
V V Bolginov**[2,4]**, V A Oboznov**[3,4]**, S V Egorov**[3,4]**, V O Shkolnikov**[4,5]**,
M J Wolf**[6]**, D Beckmann**[6] **and A V Ustinov**[1,2,3]

[1] Physikalisches Institut, Karlsruhe Institute of Technology, Wolfgang-Gaede-Str. 1, D-76131 Karlsruhe, Germany
[2] National University of Science and Technology MISiS, Leninskiy prosp. 4, Moscow, 119049, Russia
[3] Russian Quantum Center, Novaya str. 100, BC 'Ural', Skolkovo, Moscow region, 143025, Russia
[4] Institute of Solid State Physics, Russian Academy of Sciences, Chernogolovka, Moscow region, 142432, Russia
[5] Moscow Institute of Physics and Technology (State University), Institutskiy per. 9, Dolgoprudny, Moscow region, 141700, Russia
[6] Institut für Nanotechnologie, Karlsruhe Institute of Technology, D-76021 Karlsruhe, Germany

E-mail: ustinov@kit.edu

Abstract
We describe fabrication and testing of composite flux qubits combining Nb- and Al-based superconducting circuit technology. This hybrid approach to making qubits allows for employing π-phase shifters fabricated using well-established Nb-based technology of superconductor–ferromagnet–superconductor Josephson junctions. The important feature here is to obtain high interface transparency between Nb and Al layers without degrading sub-micron shadow mask. We achieve this by *in situ* Ar etching using e-beam gun. Shadow-evaporated Al/AlO$_x$/Al Josephson junctions with Nb bias pads show the expected current–voltage characteristics with reproducible critical currents. Using this technique, we fabricated composite Nb/Al flux qubits with Nb/CuNi/Nb π-shifters and measured their magnetic field response. The observed offset between the field responses of the qubits with and without π-junction is attributed to the π phase shift. The reported approach can be used for implementing a variety of hybrid Nb/Al superconducting quantum circuits.

Keywords: superconducting qubits, Josephson junctions, flux qubits, π-junctions, superconductor-ferromagnet junctions

(Some figures may appear in colour only in the online journal)

1. Introduction

One of several successfully implemented superconducting quantum circuits is a flux qubit [1, 2], which consists of a superconducting ring interrupted by three or four Josephson tunnel junctions. Though any kind of superconductor can be, in principle, taken to make a qubit, the longest coherence times for flux and other types of qubits are achieved by using shadow-evaporated aluminum as the superconducting material and naturally grown aluminum oxide on top of it as the tunnel barrier. Shadow two-angle evaporation of aluminum using a suspended electron-beam resist mask was established over thirty years ago [3, 4] and is presently the most reliable and widely used process for making sub-micron Josephson junctions. In recent years, great progress has been achieved in applying this junction manufacturing technique for superconducting quantum circuits. Two-angle evaporation process has been successfully used for a variety of

superconducting qubit types [5, 6] (charge, flux, transmon, fluxonium, etc) and appears to be most suitable for obtaining well-defined sub-micron Al/AlO$_x$/Al Josephson junctions with reliable characteristics and low density of microscopic two-level defects in the oxide tunnel barrier [7, 8]. While niobium serves as the base material for most of conventional superconducting circuits employing Nb/AlO$_x$/Nb Josephson junctions, quantum coherence times of Nb-based qubits [9–11] are significantly shorter than those of their Al-based counterparts. Aluminum superconducting flux qubits can be made very compact, while well-controlled sizes of Josephson junctions defined by two-angle evaporation make it possible engineering qubit potential with precisely defined parameters [12].

The magnetic bias needed to drive the flux qubit to its working point is a source of significant noise, leading to dephasing. The flux qubit has the most favorable operation point with minimal dephasing at the value of magnetic flux threading its loop of about $\Phi_0/2$, where Φ_0 is the magnetic flux quantum. In order to reduce the effects of external magnetic noise, it was proposed to avoid magnetic biasing by using the so-called π-junction in the qubit loop [13, 14]. The most reliable and well-established process of implementing π-junctions relies on Nb-based technology of superconductor–ferromagnet–superconductor (SFS) Josephson junctions [15]. The conventional fabrication process of π-junctions is based on the depositing of an SFS Nb/CuNi/Nb trilayer, forming the junction, followed by depositing the upper Nb wiring.

A π-junction in the superconducting loop having large enough critical current acts as a phase battery which biases the loop in the way that the phase shift on the junction is π [16]. The effect of such a phase shifter is equivalent to applying flux of $\Phi_0/2$ through the loop [17]. SFS phase shifters have already been successfully implemented in Nb-based phase qubit circuits [18], but they haven't yet been used in flux qubits. The need to combine separately made Nb and Al layers is caused by non-existing so far Al-based π-junction SFS technology, which would otherwise make it possible avoiding Nb completely. A complication arising along this development is to combine two completely separated and not easily compatible technological steps, first one for making relatively large SFS junctions based on Nb, followed by another process of manufacturing more fragile sub-micron Al junctions needed for highly-coherent flux qubits. Aluminum two-angle evaporation is performed in a separate setup, and pre-fabricated Nb structure is exposed to the air under which the natural oxide NbO$_x$ is formed on Nb surface. This complication makes the implementation of the SFS π-junction in the Al flux qubit loop challenging and requires removing the NbO$_x$ completely before the deposition of Al part of the flux qubit.

This paper is organized as follows. Section 2 describes the combined Nb/Al technology for preparation of π-qubits. In section 3, we present current–voltage measurements of Al/AlO$_x$/Al Josephson junctions with electrodes deposited on Nb pads. The developed technology allows for obtaining high quality Al/AlO$_x$/Al Josephson junctions without residual
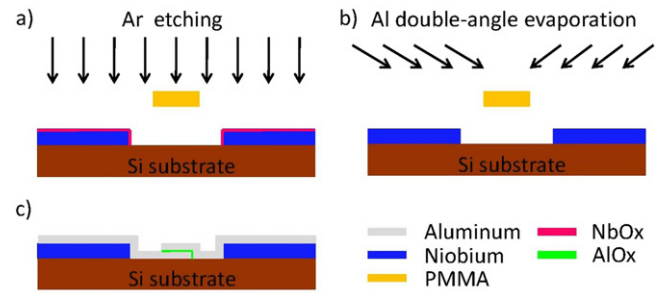

Figure 1. Fabrication process of Al/AlO$_x$/Al Josephson junctions on Nb pads. (a) Etching of NbO$_x$ with the directed Ar beam *in situ* right before the deposition of Al. (b) Double-angle Al shadow evaporation. (c) Resulting structure of Al Josephson junction on Nb pads free from NbO$_x$ after the lift-off procedure.

resistance at Nb/Al interface. In section 4, we present measurements of flux qubits with Nb/CuNi/Nb π-junctions.

2. Fabrication

As the starting point, we describe our fabrication process of Al/AlO$_x$/Al Josephson junctions with the Nb contact pads. Schematically, the process is shown on figure 1. Prior applying this process, Nb pads are fabricated in a separate vacuum chamber. The main difficulty for achieving a good superconducting contact between Nb and Al here is caused by a layer of non-superconducting NbO$_x$, formed on the surface of Nb due to exposure to the air between the two processes.

The Nb contact pad layer was deposited by dc magnetron sputtering and its patterning was done with the help of conventional optical lithography. After that the sample was covered by a double-layer resist and exposed in an electron-beam lithography machine to define the desired structure for the following double-angle evaporation of Al. Upon transferring the sample to Al deposition chamber, the surface layer of NbO$_x$ was etched away *in situ* using the directed Ar beam in order to create a clean Nb surface before deposition of Al. The specific data for interface transparency after Ar-cleaning of Nb-surface could be found in [15], for example.

Several measures for the etching procedure were taken aiming at preventing the resist pattern from melting. We precooled the sample for 1 h in a main chamber of evaporation machine at a high vacuum of 10^{-9} mbar at the temperature of about $T \approx -120\,°C$. The layer of NbO$_x$ was etched away in the load-lock by the directed Ar beam in four periods of 30 s each, interrupted by 1 min pauses. After that, the aluminum Josephson junctions were deposited using the standard double-angle shadow evaporation and oxidation [3, 4]. We found out that the Ar beam current density of $20\,\mu A\,cm^{-2}$ was sufficient to etch down the NbO$_x$ layer and establish the superconducting contact between Al and Nb. The whole fabrication process is shown in figure 1.

We fabricated a series of Al/AlO$_x$/Al Josephson junctions having the dimensions $0.2 \times 1.0\,\mu m^2$. Furthermore, the flux qubits interrupted by three Josephson junctions of this kind were fabricated. The dimensions of Josephson junctions in
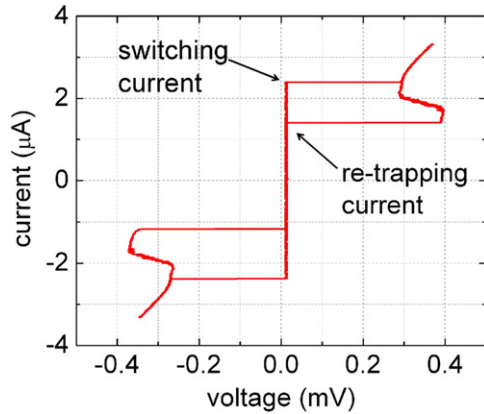
Figure 2. Typical current–voltage characteristics of a hybrid Nb/Al/AlO$_x$/Al/Nb Josephson junctions having the dimensions $0.2 \times 1.0 \, \mu m^2$. The re-trapping current 'back-bending' is explained by the self-heating.

flux qubits were $0.2 \times 0.5 \, \mu m^2$ for the two junctions and $0.2 \times 0.335 \, \mu m^2$ for the smaller α-junction aiming at $\alpha = 0.67$ [1, 2].

3. Characterization of Al/AlO$_x$/Al Josephson junctions

Fabricated samples were measured in vacuum attached to a sample holder of a He-3 cryostat and cooled down to a temperature of 300 mK. The current–voltage characteristics were measured using a four-point configuration in the current-bias mode. Figure 2 shows typical *IV*-curve for one of the test Al/AlO$_x$/Al junctions having the dimensions $0.2 \times 1.0 \, \mu m^2$. One can see a clear supercurrent branch as high as $2.5 \, \mu A$. Switching current values of $2 \pm 0.54 \, \mu A$ and re-trapping currents of around $1 \pm 0.25 \, \mu A$ were measured for junctions made on several chips. According to the process described above, all the contact pads of our junctions are made of niobium so that each lead contained Nb/Al interface. The current–voltage characteristics of Al/AlO$_x$/Al Josephson junctions showed no evidence of any residual resistance due to Nb/Al interfaces. So thus the quality of the fabricated Nb/Al/AlO$_x$/Al/Nb hybrid structures is high enough for implementation in quantum circuits.

From the topology of the junctions we estimated the junction capacitance $C \approx 4.43 \pm 0.92 \, fF$. The pronounced 'back-bending' of the re-trapping current branch visible in figure 2 is rather typical for vacuum-based transport measurements of small aluminum junctions in this range of the critical current density and can be explained by non-equilibrium effects due to the junction self-heating. Same phenomenon is also responsible for about 20% reduction in the measured value of the gap voltage V$_g$ [19].
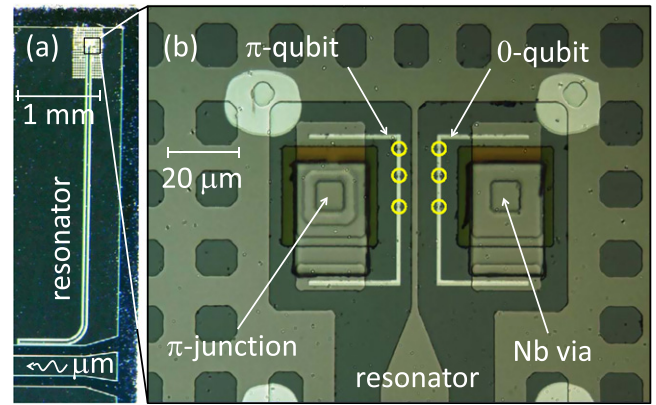

Figure 3. (a) $\lambda/4$ resonator capacitively coupled to the transmission line. (b) Optical picture of the two composite Nb/Al flux qubits placed near the shorted end of the $\lambda/4$ resonator. Nb part of the left qubit contains the π-junction. Right qubit has Nb 'via' structure forming a superconducting short. The circles mark the positions of aluminum Josephson junctions.

4. Flux qubit measurements

SFS π-junction fabrication technology is described in detail in [20]. The fabrication process employed in this study differs from previous works. Here, all layers were deposited in the beginning of the process in a single vacuum cycle and then patterned using photo-lithography, reactive and argon ion etching, followed by magnetron sputtering and thermal evaporation. We have studied the dependence of critical current density on the CuNi-layer thickness using this technology [21] and discovered that it results in critical currents one order of magnitude larger than the technology used earlier [15].

For measurements of the flux qubits we used the conventional dispersive readout setup discussed in detail elsewhere [12]. Two flux qubits were placed near the shorted end of the $\lambda/4$ resonator, one with the SFS π-junction with 12 nm layer of Cu$_{0.47}$Ni$_{0.53}$ [15], and another one without it. The opposite open end of the resonator was capacitively coupled to an on-chip coplanar waveguide. The micrograph, shown in figure 3, illustrates the sample.

The magnetic flux through the qubit loops was applied by using an external magnetic bias coil. Measurements were performed in a dilution cryostat at the base temperature of 25 mK. We swept electrical current through the bias coil, thus changing the flux through the qubit loops. Simultaneously, the resonator was probed at its fundamental $\lambda/4$ mode frequency ω_r with a microwave signal transmitted and detected via a vector network analyzer. We measured the amplitude and phase responses of the probe signal amplified with a low-noise cryogenic amplifier at a fixed frequency $\omega_r/(2\pi) = 10.218 \, GHz$.

In the employed dispersive readout scheme, the resonator acquires a dispersive shift due to the coupling to the qubit
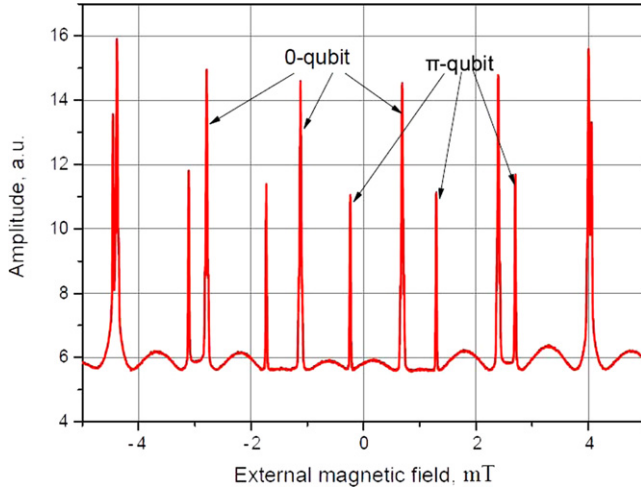
Figure 4. Amplitude of the dispersive response measured with a probe signal through a transmission line at a fixed frequency $\omega = \omega_r = 10.218$ GHz. A periodic pattern with peaks of larger amplitude corresponds to the flux qubit without π-junction, while smaller peaks are referred to the flux qubit with π-junction. The difference in amplitudes of the signals is attributed to the different coupling and detuning of the qubits from the resonator.

[22, 23]

$$\Delta\omega_r = \pm \frac{\tilde{g}}{\omega_q - \omega_r}, \tag{1}$$

where $\tilde{g}$ is an effective coupling of the resonator to the qubit, ω_q is the transition frequency between the $|0\rangle$ and $|1\rangle$ qubit states, ω_r is the resonant frequency of the unperturbed resonator. From equation (1) one can see that, for the qubit far-detuned from the resonator frequency, the dispersive shift is small. When the qubit frequency ω_q approaches the resonator frequency ω_r, a relatively large dispersive shift $\Delta\omega_r$ occurs.

For the flux qubit with the π-junction, we made the critical current of the π-junction much larger than the critical current that of any Al/AlO$_x$/Al Josephson junctions forming the qubit. The following parameters have been used for Nb/Cu$_{0.47}$Ni$_{0.53}$/Nb π-junction: CuNi-layer thickness of 12 nm, critical current density of 3.7 kA cm^{-2} [21], mesa size $10 \times 10\,\mu$m^2, and the estimated critical current of about 3.7 mA. The value of SFS-junctions critical current was about three orders in magnitude larger than for tunnel junctions. In this case, due to relatively small persistent current flowing in the qubit loop, the phase difference across the π-junction remains always close to π, even at zero magnetic field. That causes the phase drop across aluminum tunnel junctions of the qubit to be shifted by the value of π, that is equivalent to applying flux $\Phi_0/2$ in the qubit loop. Two qubits in our experiment can be distinguished and measured simultaneously with a single resonator because of their slightly different loop areas and coupling strengths ($\tilde{g}_1$ and $\tilde{g}_2$) to the resonator, provided by different distances between the qubit loops and the resonator wire, see figure 3.

The field response of the resonator coupled to two flux qubits, one with and another without π-shifter is shown in figure 4. A peak in the transmitted microwave amplitude
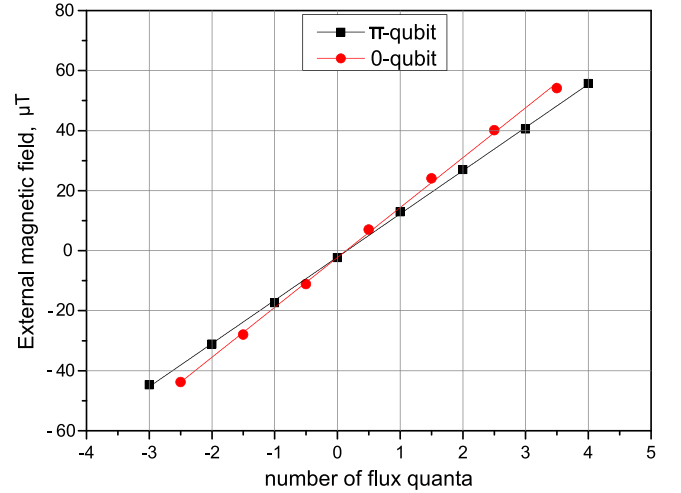

Figure 5. The magnetic field bias versus flux quanta per qubit loop, extracted from positions of peaks in figure 4. The horizontal axis offset is chosen to have peaks of π-qubit at integer values of Φ/Φ_0.

occurs when the frequency of the transition between the ground and excited state of one of either qubit ω_{q1} or ω_{q2} approaches the resonator frequency ω_r, which occurs at the magnetic flux values close to $\Phi_0/2 \pm n\Phi_0$ for the qubit without π-junction and at $\pm n\Phi_0$ for the qubit with π-junction, where n is an integer.

Next, we need to sort out two families of periodic peaks in figure 4, one of them corresponding to 0-qubit and another to π-qubit. This procedure is not straightforward because of non-ideal magnetic shielding. Indeed, one can see from figure 4 that there is no peak exactly at zero magnetic field, indicating the presence of residual magnetic field in the setup. In figure 5, we have plotted the positions of peaks as as a function of magnetic flux, for data in a broader flux range, taken in the same measurement as figure 4. We assumed that a period for each peak family is one flux quantum, the residual flux of less than one flux quantum and the nearest-to-zero peak as corresponding to π-qubit. One can see that both peak families could be approximated by linear dependencies, each having its own slope, and the intersection between two families takes place at zero net magnetic field. The difference in slopes is due to different mutual inductances between qubits and external coil. An intersection point has to correspond to zero magnetic flux, at which the π-qubit should display here a peak in the dispersive signal. Under this assumption, the residual magnetic field is equal to approximately $2\,\mu$T and the residual magnetic flux is less than one flux quantum. One can easily identify two periods of oscillations in figure 4. We suppose that the smaller period of the π-junction qubit oscillations in the applied magnetic field can be associated with an additional Josephson inductance of its loop induced by the π-junction. The smaller peak amplitude of the π-junction qubit response can be related to a larger detuning of its gap frequency from the resonator frequency, as well as to the additional inductance mentioned above. The energy gap of a flux qubit is extremely hard to control due to

its very sensitive dependence on the relation between critical currents for three aluminum junctions.

It is important to discuss the uniqueness of π-qubit response identification. Actual values of magnetic flux in figure 5 are assigned with possible offset by an integer number of flux quanta. However, this circumstance doesn't alter our definition of 0- and π-qubit responses. Indeed, an offset in definition of zero-flux peak shifts *all* points of *both* peak families in figure 5 along the horizontal axis by an integer value. In this case, the crosspoint flux value will change but it will remain to be integer-valued and the same peak will correspond to the crosspoint. While our definition of zero magnetic flux is just an assumption, the identification of π-qubit peaks base on the above described arguments seems unambiguous.

5. Conclusion

In conclusion, we developed a fabrication process which allows to create a superconducting interface between Nb and Al thin films produced in different technological processes. The developed procedure features pre-cooling and Ar etching procedure of oxidized Nb surface *in situ*, before deposition of Al/AlO$_x$/Al Josephson junctions using a standard double-angle shadow evaporation. This process can also be implemented for more complex Nb/Al qubit circuits. Hybrid Al/AlO$_x$/Al flux qubits containing Nb/Cu$_{0.47}$Ni$_{0.53}$/Nb π-shifters were fabricated using the developed approach. We observed the field response of two flux qubits (one with and another without π-shifter) coupled to the same λ/4 resonator. The magnetic field shift between two periodic qubit oscillation patterns measured at mK temperatures indicates the expected π-junction phase bias in one of the flux qubit loops. The use of the π-shifter makes it possible to avoid magnetic biasing, normally needed for reaching the most favorable flux qubit operating point, and thus to reduce unavoidable variations of magnetic bias between different qubits on chip.

Acknowledgments

References

[1] Mooij J E, Orlando T P, Levitov L, Tian L, van der Wal C H and Lloyd S 1999 *Science* **285** 1036
[2] Chiorescu I, Nakamura Y, Harmans C J P M and Mooij J E 2003 *Science* **299** 1869
[3] Niemeyer J 1974 *PTB Mitt.* **84** 251
[4] Dolan G J 1977 *Appl. Phys. Lett.* **31** 337
[5] Clarke J and Wilhelm F K 2008 *Nature* **453** 1031
[6] You J and Nori F 2011 *Nature* **474** 589
[7] Lupascu A, Bertet P, Driessen E F C, Harmans C J P M and Mooij J E 2009 *Phys. Rev.* B **80** 172506
[8] Martinis J M 2009 *Quantum Inf. Process.* **8** 81
[9] Lee J C, Oliver W D, Berggren K K and Orlando T P 2007 *Phys. Rev.* B **75** 144505
[10] Lisenfeld J, Lukashenko A, Ansmann M, Martinis J M and Ustinov A V 2007 *Phys. Rev. Lett.* **99** 170504
[11] Hoskinson E, Lecocq F, Didier N, Fay A, Hekking F W, Guichard W, Buisson O, Dolata R, Mackrodt B and Zorin A B 2009 *Phys. Rev. Lett.* **102** 097004
[12] Jerger M, Poletto S, Macha P, Huebner U, Lukashenko A, Il'ichev E and Ustinov A V 2011 *Eur. Phys. Lett.* **96** 40012
[13] Ioffe L B, Geshkenbein V B, Feigelman M V, Fauchere A L and Blaetter G 1999 *Nature* **398** 679
[14] Blatter G, Geshkenbein V B and Ioffe L B 2001 *Phys. Rev.* B **63** 174511
[15] Oboznov V A, Bolginov V V, Feofanov A K, Ryazanov V V and Buzdin A I 2006 *Phys. Rev. Lett.* **96** 197003
[16] Frolov S M, Stoutimore M J A, Crane T A, Van Harlingen D J, Oboznov V A, Ryazanov V V, Ruosi A, Granata C and Russo M 2008 *Nat. Phys.* **4** 32
[17] Ustinov A V and Kaplunenko V K 2003 *J. Appl. Phys.* **94** 5405
[18] Feofanov A K *et al* 2010 *Nature Phys.* **6** 593
[19] Lotkov S V, Tolkacheva E M, Balashov D V, Khabirov M I, Buchholz F-I and Zorin A B 2006 *Appl. Phys. Lett.* **89** 132115
[20] Bol'ginov V V, Stolyarov V S, Sobanin D S, Karpovich A L and Ryazanov V V 2012 *JETP Lett.* **95** 366
[21] Oboznov V A *et al* 2014 in preparation
[22] Blais A, Huang R-S, Wallraff A, Girvin S M and Schoelkopf R J 2004 *Phys. Rev.* A **69** 062320
[23] Wallraff A, Schuster D I, Blais A, Frunzio L, Huang R-S, Majer J, Kumar S, Girvin S M and Schoelkopf R J 2004 *Nature* **431** 162